Modeling of the dynamic characteristic of viscoelastic dielectric elastomer actuators subject to different conditions of mechanical load

Cite as: J. Appl. Phys. **117**, 084902 (2015); https://doi.org/10.1063/1.4913384
Submitted: 17 November 2014 . Accepted: 11 February 2015 . Published Online: 25 February 2015

Junshi Zhang, Liling Tang, Bo Li, Yanjie Wang, and Hualing Chen

Modeling of the dynamic characteristic of viscoelastic dielectric elastomer actuators subject to different conditions of mechanical load

Junshi Zhang,[1,2,3] Liling Tang,[1,2,4] Bo Li,[1,5] Yanjie Wang,[1,5] and Hualing Chen[1,5,a)]
[1]*State Key Laboratory for Strength and Vibration of Mechanical Structures, Xi'an Jiaotong University, Xi'an 710049, China*
[2]*School of Aerospace, Xi'an Jiaotong University, Xi'an 710049, China*
[3]*Department of Materials Science and Engineering, Henry Samueli School of Engineering and Applied Science, University of California, Los Angeles, California 90095, USA*
[4]*Department of Mechanical Engineering, The Hong Kong Polytechnic University, Hung Hom, Kowloon, Hong Kong*
[5]*School of Mechanical Engineering, Xi'an Jiaotong University, Xi'an 710049, China*

(Received 17 November 2014; accepted 11 February 2015; published online 25 February 2015)

Subject to a mechanical load or a voltage, a membrane of a dielectric elastomer deforms. As for the deformation mode, the dynamic performance and stability are strongly affected by how mechanical forces are applied. In the current study, by using the Euler-Lagrange equation, an analytical model is developed to characterize the dynamic performance of a homogeneously deformed viscoelastic dielectric elastomer under the conditions of equal-biaxial force, uniaxial force, and pure shear state, respectively. Numerical results are shown to describe the electromechanical deformation and stability. It is observed that the resonant frequency (where the amplitude-frequency curve peaks) has dependencies on the deformation mode, the level of mechanical load, and the applied electric field. When a dielectric elastomer membrane is subject to equal-biaxial force or pure shear state, it undergoes a nonlinear quasi-periodic vibration. An aperiodic motion of the dielectric elastomer system is induced by the boundary condition of a uniaxial force. © *2015 AIP Publishing LLC*.
[http://dx.doi.org/10.1063/1.4913384]

I. INTRODUCTION

Subject to a voltage through the thickness direction, a membrane of a dielectric elastomer (DE) shrinks in thickness and expands in area.[1–6] Because of its unique features like fast response time, large deformation, lightweight and high energy density, a DE has been considered for high performance applications, such as soft robots,[7,8] MEMS,[9–11] tunable lenses,[12–14] loudspeaker,[15] and power generators for harvesting energy.[16–18]

Most of the present studies on DE are focused on quasi-static deformation.[3,5,6] Nonlinear modeling and the stability analysis of DE in quasi-static deformation have been documented and developed in various forms.[19–22] Generally speaking, there are three different in-plane deformation modes of DE, including equal-biaxial force, uniaxial force, and pure shear state. The investigation on the static characteristic of DE under the three modes was reported recently.[23,24] The equal-biaxial and uniaxial modes will induce the pull-in instability, while the pure shear mode is able to provide a giant deformation before the wrinkling instability.[24]

However, to perform as electromechanical actuators, e.g., frequency tuning,[25] pumps,[26] and acoustic actuators,[27] a DE is mostly expected to operate under the alternating load in applications, where inertia force plays an important role. Recently, researchers carried out the modeling of the nonlinear dynamic performance of DE taking into account different configurations, such as membrane,[25,28–30] micro-beam resonator,[31] Haptics In a Can (HIC) slide actuator,[32] balloon,[33,34] and spherical shell.[35] The DE-based structures, including membrane, micro-beam resonator, and HIC slide actuator undergo the in-plane deformation, while the DE balloon and DE spherical shell present the out-of-plane deformation. Although the dynamics of DE with various shapes was studied significantly, the general study on the dynamic behavior and the dynamic stability under the three different in-plane deformation modes (equal-biaxial force, uniaxial force, and pure shear state) is still lacking.

Majority of the current dynamic works were carried out by the method of virtual work.[28,30,32–34] Recently, Xu *et al.*[29] and Sheng *et al.*,[36] respectively, proposed an analytical model from the Euler-Lagrange equation to research the dynamic performance of a homogeneously deformed DE actuator merely under the action of electric field. The Euler-Lagrange equation can be employed to solve the problem of the nonlinear dynamics with multiple degrees-of-freedom (DOFs) commendably. Unfortunately, they did not take into consideration the effect of the mechanical load. However, as an actuator, a DE must be connected to the external environment and undergo a mechanical load. As mentioned before, there are three different conditions of mechanical load, and a DE has to vary the deformation mode to acclimatize itself to the force outside. Thus, study on the conditions of mechanical load of DE and how it affects DE's dynamic electromechanical performance is necessary and expected.

Furthermore, most of the DE materials, such as VHB, exhibit a strong viscoelasticity and the charge leakage through the thickness direction.[4,36–45] Viscoelasticity allows

a)Author to whom correspondence should be addressed. Electronic mail: hlchen@mail.xjtu.edu.cn

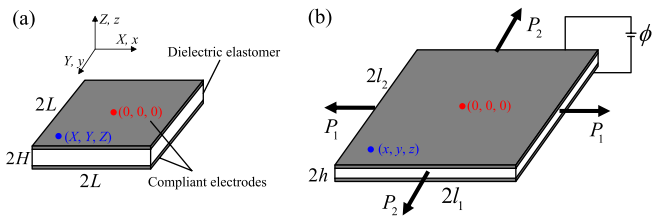

FIG. 1. Schematic of a square DE membrane. (a) In the reference state, subject to no force and no voltage, a square DE membrane is of lengths $2L$ and $2L$, and thickness $2H$. (b) In the deformed state, subject to the biaxial forces P_1 and P_2 and a voltage ϕ, the membrane is of lengths $2l_1$ and $2l_2$, and thickness $2h$. The coordinate of material point (X, Y, Z) in the reference state deforms to (x, y, z) in the deformed state, with the original point $(0, 0, 0)$ fixed in the center.

the deformation to have a significant time-dependence,[37–40,42–44] while the charge leakage induces the corresponding current leakage through the membrane.[4,37–40,45] Both of them demonstrated an obvious influence on the electromechanical performance of DE. Viscoelasticity dissipates the mechanical energy, suppressing the amplitude of vibration (including the amplitude of resonant frequency).[34,36] In this paper, we use the electrical field as the input parameters and investigate how it affects the dynamic performance of DE. When the electrical field is a specific value, the induced Maxwell stress is also determined although the charge leakage is always companied. The induced Maxwell stress can guarantee a corresponding vibration that is independent to the charge leakage, as Fig. 11 in the work reported by Foo *et al.*[37] In other words, the charge leakage does not affect the dynamic performance of DE actuators under the actuation of electrical field. Consequently, the charge leakage is not included in the developed viscoelastic model of DE in this paper.

By using the Euler-Lagrange equation, we made a theoretical prediction of the dynamic electromechanical response of a viscoelastic DE membrane subject to three different conditions of mechanical load: equal-biaxial force, uniaxial force, and pure shear state. We then applied the model to investigate the effects of the mechanical force and the applied electric field on the dynamic characteristic of DE actuator under these three deformation modes, respectively. Subsequently, we analyzed the dynamic stability at special frequencies by the phase paths and the Poincaré maps.

II. DYNAMICS MODEL OF A VISCOELASTIC DE MEMBRANE

Subject to a mechanical force or a voltage, a membrane of a DE deforms. Fig. 1(a) illustrates a square DE membrane of lengths $2L$ and $2L$, and thickness $2H$ in the reference state. In the deformed state, when the forces P_1 and P_2 are applied in the plane and the two electrodes are subject to a voltage ϕ, the membrane is of lengths $2l_1$ and $2l_2$, and thickness $2h$. Define the stretches as $\lambda_1 = l_1/L$, $\lambda_2 = l_2/L$, and $\lambda_3 = h/H$. Based on continuum mechanics, the material coordinate (X, Y, Z) labels a certain material point in the reference state, while the coordinate (x, y, z) denotes the deformable material point corresponding to the material point (X, Y, Z). We assume that the middle plane of the membrane $(0, 0, 0)$ shows no normal displacement.[29,36] For a membrane of an incompressible elastomer ($\lambda_3 = \lambda_1^{-1}\lambda_2^{-1}$), the motion of the body can be written as

$$x = \lambda_1 X \quad y = \lambda_2 Y \quad z = \lambda_1^{-1}\lambda_2^{-1} Z. \tag{1}$$

The governing equation is obtained by the Euler-Lagrange equation

$$\frac{\partial \ell}{\partial \lambda_i} - \frac{\mathrm{d}}{\mathrm{d}t}\left(\frac{\partial \ell}{\partial \dot{\lambda}_i}\right) = 0, \quad \ell = T - \Pi \quad i = 1, 2, \tag{2}$$

where $\dot{\lambda}_i$ denotes the rate of change of λ_i, ℓ is the Lagrange, T is the kinetic energy, Π is the potential of the conservative forces in the system.

The kinetic energy takes the form[29]

$$T = \int_\Omega \frac{1}{2}\rho\left(\dot{x}^2 + \dot{y}^2 + \dot{z}^2\right)\mathrm{d}\Omega, \tag{3}$$

where ρ is the density of the elastomer, Ω is the domain occupied by the deformed configuration, $\dot{x}$, $\dot{y}$, and $\dot{z}$ are the velocities in three directions, respectively.

The DE membrane is approximately simulated by a previously developed rheological model[36–40,42–44] with two parallel units: unit A consists of a spring α which deforms reversibly; and unit B consists of another spring β with a series-wound dashpot that relaxes in time and dissipates the energy, as sketched in Fig. 2. Note that the free energy of the system consists of the elastic energy, for which the Neo-Hookean model[29,36,39,40,43] is used, the potential energy induced by the mechanical forces, and the electrostatic energy. Because of the homogeneity, the potential Π in the system is obtained by multiplying the free energy density with the volume[29,36,46]

$$\begin{aligned}\Pi = 8HL^2\Bigg[&\frac{\mu^\alpha}{2}\left(\lambda_1^2 + \lambda_2^2 + \lambda_1^{-2}\lambda_2^{-2} - 3\right)\\ &+ \frac{\mu^\beta}{2}\left(\lambda_1^2\xi_1^{-2} + \lambda_2^2\xi_2^{-2} + \lambda_1^{-2}\lambda_2^{-2}\xi_1^2\xi_2^2 - 3\right)\\ &- \frac{P_1}{4HL}\lambda_1 - \frac{P_2}{4HL}\lambda_2 - \frac{\varepsilon}{2}E^2\lambda_1^2\lambda_2^2\Bigg]\end{aligned} \tag{4}$$

in which ε is the permittivity of the elastomer, μ^α and μ^β are the shear moduli of spring α and spring β, respectively, $E = \phi/2H$ is the normal electric field, ξ_1 and ξ_2 are the nonelastic stretches due to the dashpot in directions x and y. For spring β, the state of deformation is characterized by a different stretch λ_i^e, determined by a well-established multiplication rule as $\lambda_i^e = \lambda_i/\xi_i$.[36–40,42–44] The rate of deformation in the dashpot (regarded as a Newtonian fluid) is described by

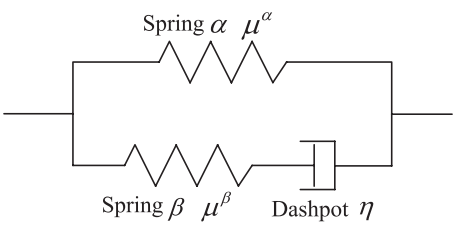

FIG. 2. Viscoelastic model of DE with two parallel units: unit A consists of a spring α, unit B consists of another spring β and a serious-wound dashpot.

$\xi_1^{-1}\mathrm{d}\xi_1/\mathrm{d}t$ and $\xi_2^{-1}\mathrm{d}\xi_2/\mathrm{d}t$, and the relationship between the rate of deformation and the stress can be written as[37,43]

$$\frac{\mathrm{d}\xi_1}{\mathrm{d}t} = \frac{\xi_1}{3\eta}\left[\mu^\beta\left(\lambda_1^2\xi_1^{-2} - \lambda_1^{-2}\lambda_2^{-2}\xi_1^2\xi_2^2\right) - \frac{\mu^\beta}{2}\left(\lambda_2^2\xi_2^{-2} - \lambda_1^{-2}\lambda_2^{-2}\xi_1^2\xi_2^2\right)\right], \tag{5}$$

$$\frac{\mathrm{d}\xi_2}{\mathrm{d}t} = \frac{\xi_2}{3\eta}\left[\mu^\beta\left(\lambda_2^2\xi_2^{-2} - \lambda_1^{-2}\lambda_2^{-2}\xi_1^2\xi_2^2\right) - \frac{\mu^\beta}{2}\left(\lambda_1^2\xi_1^{-2} - \lambda_1^{-2}\lambda_2^{-2}\xi_1^2\xi_2^2\right)\right], \tag{6}$$

where η is the viscosity of the dashpot. The viscoelastic relaxation time, τ_v, is prescribed as the value between η and μ^β, $\tau_v = \eta/\mu^\beta$.[36–40,42–44]

As reported before, there are three different in-plane deformation modes of DE, including equal-biaxial force, uniaxial force, and pure shear state.[23,24] In the following, modeling of a DE membrane under the three different conditions of mechanical load is considered, respectively.

A. Model of a DE membrane under equal-biaxial force

Consider the dynamic characteristic of a viscoelastic DE membrane under the condition of equal-biaxial force ($P_1 = P_2 = P$), as shown in Fig. 3(b). Subject to equal-biaxial force and a voltage, the membrane has stretches $\lambda_1 = \lambda_2 = \lambda_{EB}$, $\xi_1 = \xi_2 = \xi_{EB}$. Thus, the kinetic energy is derived from Eq. (3) as

$$T = \frac{8}{3}\rho L^4 H\dot{\lambda}_{EB}^2 + \frac{16}{3}\rho L^2 H^3\frac{\dot{\lambda}_{EB}^2}{\lambda_{EB}^6}, \tag{7}$$

and the potential is obtained from Eq. (4) as

$$\Pi = 8HL^2\left[\frac{\mu^\alpha}{2}\left(2\lambda_{EB}^2 + \lambda_{EB}^{-4} - 3\right) + \frac{\mu^\beta}{2}\left(2\lambda_{EB}^2\xi_{EB}^{-2} + \lambda_{EB}^{-4}\xi_{EB}^4 - 3\right) - \frac{P}{2HL}\lambda_{EB} - \frac{\varepsilon}{2}E^2\lambda_{EB}^4\right]. \tag{8}$$

Substituting Eqs. (7) and (8) into the Euler-Lagrange equation (2), we obtain the governing equation under the condition of equal-biaxial force

$$\ddot{\lambda}_{EB} - \frac{6}{\lambda_{EB}(2 + L^2H^{-2}\lambda_{EB}^6)}\dot{\lambda}_{EB}^2 + \frac{3}{\rho H^2(2 + L^2H^{-2}\lambda_{EB}^6)} \times \left[\mu^\alpha\left(\lambda_{EB}^7 - \lambda_{EB}\right) + \mu^\beta\left(\lambda_{EB}^7\xi_{EB}^{-2} - \lambda_{EB}\xi_{EB}^4\right) - \frac{P}{4HL}\lambda_{EB}^6 - \varepsilon E^2\lambda_{EB}^9\right] = 0. \tag{9}$$

The rate of deformation due to the dashpot under the condition of equal-biaxial force can be simplified by Eqs. (5) and (6) as

$$\frac{\mathrm{d}\xi_{EB}}{\mathrm{d}t} = \frac{\mu^\beta}{6\eta}\left(\lambda_{EB}^2\xi_{EB}^{-1} - \lambda_{EB}^{-4}\xi_{EB}^5\right). \tag{10}$$

B. Model of a DE membrane under uniaxial force

In the following, we consider the dynamic characteristic of a viscoelastic DE membrane under the condition of uniaxial force ($P_1 = P$, $P_2 = 0$), as shown in Fig. 3(c). Subject to a uniaxial force in the x-direction and a voltage, the membrane has stretches λ_{UA1}, λ_{UA2}, ξ_{UA1}, and ξ_{UA2}, respectively. The kinetic energy of this system is derived from Eq. (3) based on the 2-DOFs as

$$T = \frac{4}{3}\rho L^4 H\dot{\lambda}_{UA1}^2 + \frac{4}{3}\rho L^4 H\dot{\lambda}_{UA2}^2 + \frac{4}{3}\rho L^2 H^3\lambda_{UA1}^{-2}\lambda_{UA2}^{-2}\left(\lambda_{UA1}^{-2}\dot{\lambda}_{UA1}^2 + \lambda_{UA2}^{-2}\dot{\lambda}_{UA2}^2 + 2\lambda_{UA1}^{-1}\lambda_{UA2}^{-1}\dot{\lambda}_{UA1}\dot{\lambda}_{UA2}\right), \tag{11}$$

and the potential is gained from Eq. (4) as

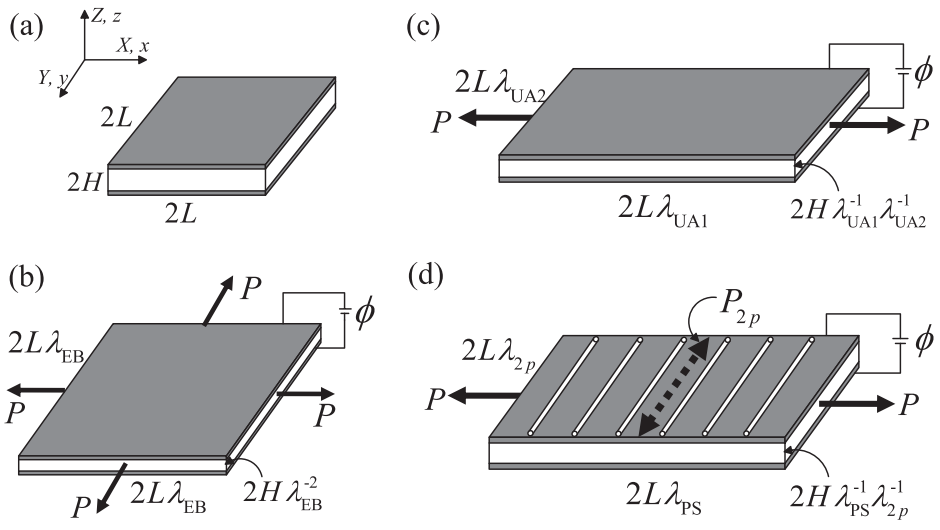

FIG. 3. (a) In the reference state, subject to no force and no voltage, a DE membrane has dimensions $2L\times2L\times2H$. In the deformed state, (b) subject to equal-biaxial force P in the plane and a voltage ϕ, the membrane has stretches $\lambda_1 = \lambda_2 = \lambda_{EB}$ and $\xi_1 = \xi_2 = \xi_{EB}$; (c) subject to uniaxial force P in x-direction and a voltage ϕ, the membrane has stretches λ_{UA1}, λ_{UA2}, ξ_{UA1}, and ξ_{UA2}; (d) the stretch in y-direction is constrained as $\lambda_2 = \lambda_{2p}$, and the level of the force to constrain $\lambda_2 = \lambda_{2p}$ is denoted by P_{2p}; subject to the force P in x-direction and a voltage ϕ, the membrane has stretches $\lambda_1 = \lambda_{PS}$ and $\xi_1 = \xi_{PS}$.

$$\Pi = 8HL^2\left[\frac{\mu^\alpha}{2}\left(\lambda_{UA1}^2+\lambda_{UA2}^2+\lambda_{UA1}^{-2}\lambda_{UA2}^{-2}-3\right)+\frac{\mu^\beta}{2}\left(\lambda_{UA1}^2\xi_{UA1}^{-2}+\lambda_{UA2}^2\xi_{UA2}^{-2}+\lambda_{UA1}^{-2}\lambda_{UA2}^{-2}\xi_{UA1}^2\xi_{UA2}^2-3\right)\right.$$
$$\left.-\frac{P}{4HL}\lambda_{UA1}-\frac{\varepsilon}{2}E^2\lambda_{UA1}^2\lambda_{UA2}^2\right]. \tag{12}$$

Substituting Eqs. (11) and (12) into the Euler-Lagrange equation (2), we obtain the governing equations under the condition of uniaxial force

$$\frac{8}{3}\rho L^2H^3\left[\left(L^2H^{-2}+\lambda_{UA1}^{-4}\lambda_{UA2}^{-2}\right)\ddot{\lambda}_{UA1}+\lambda_{UA1}^{-3}\lambda_{UA2}^{-3}\ddot{\lambda}_{UA2}\right]-\frac{16}{3}\rho L^2H^3\left(\lambda_{UA1}^{-5}\lambda_{UA2}^{-2}\dot{\lambda}_{UA1}^2+\lambda_{UA1}^{-4}\lambda_{UA2}^{-3}\dot{\lambda}_{UA1}\dot{\lambda}_{UA2}+\lambda_{UA1}^{-3}\lambda_{UA2}^{-4}\dot{\lambda}_{UA2}^2\right)$$
$$+8HL^2\left[\mu^\alpha\left(\lambda_{UA1}-\lambda_{UA1}^{-3}\lambda_{UA2}^{-2}\right)+\mu^\beta\left(\lambda_{UA1}\xi_{UA1}^{-2}-\lambda_{UA1}^{-3}\lambda_{UA2}^{-2}\xi_{UA1}^2\xi_{UA2}^2\right)-\frac{P}{4HL}-\varepsilon E^2\lambda_{UA1}\lambda_{UA2}^2\right]=0, \tag{13}$$

$$\frac{8}{3}\rho L^2H^3\left[\left(L^2H^{-2}+\lambda_{UA1}^{-2}\lambda_{UA2}^{-4}\right)\ddot{\lambda}_{UA2}+\lambda_{UA1}^{-3}\lambda_{UA2}^{-3}\ddot{\lambda}_{UA1}\right]-\frac{16}{3}\rho L^2H^3\left(\lambda_{UA1}^{-2}\lambda_{UA2}^{-5}\dot{\lambda}_{UA2}^2+\lambda_{UA1}^{-3}\lambda_{UA2}^{-4}\dot{\lambda}_{UA1}\dot{\lambda}_{UA2}+\lambda_{UA1}^{-4}\lambda_{UA2}^{-3}\dot{\lambda}_{UA1}^2\right)$$
$$+8HL^2\left[\mu^\alpha\left(\lambda_{UA2}-\lambda_{UA1}^{-2}\lambda_{UA2}^{-3}\right)+\mu^\beta\left(\lambda_{UA2}\xi_{UA2}^{-2}-\lambda_{UA1}^{-2}\lambda_{UA2}^{-3}\xi_{UA1}^2\xi_{UA2}^2\right)-\varepsilon E^2\lambda_{UA1}^2\lambda_{UA2}\right]=0. \tag{14}$$

The rate of deformation due to the dashpot under the condition of uniaxial force can be received based on Eqs. (5) and (6)

$$\frac{d\xi_{UA1}}{dt}=\frac{\mu^\beta}{6\eta}\left(2\lambda_{UA1}^2\xi_{UA1}^{-1}-\lambda_{UA2}^2\xi_{UA2}^{-2}\xi_{UA1}-\lambda_{UA1}^{-2}\lambda_{UA2}^{-2}\xi_{UA1}^3\xi_{UA2}^2\right), \tag{15}$$

$$\frac{d\xi_{UA2}}{dt}=\frac{\mu^\beta}{3\eta}\left(2\lambda_{UA2}^2\xi_{UA2}^{-1}-\lambda_{UA1}^2\xi_{UA1}^{-2}\xi_{UA2}-\lambda_{UA1}^{-2}\lambda_{UA2}^{-2}\xi_{UA1}^2\xi_{UA2}^3\right). \tag{16}$$

C. Model of a DE membrane under pure shear state

By contrast, the giant deformation in a certain direction has been observed when the deformation in the other in-plane direction is constrained.[23,24] The stiff fibers are employed to constrain a certain in-plane direction in experiments, as reported by Lu *et al.*[23] Here, we constrain the y-directional deformation and prescribe the stretch as $\lambda_2=\lambda_{2p}$. Next consider the dynamic characteristic of a viscoelastic DE membrane under a pure shear state, as shown in Fig. 3(d). Subject to a force in x-direction and a voltage, the membrane has stretches λ_1 and ξ_1 in x-direction. Due to the constrained stretch in y-direction $\lambda_2=\xi_2=\lambda_{2p}=\xi_{2p}$, $\dot{\lambda}_2=0$ can be acquired consequently. By defining $\lambda_1=\lambda_{PS}$ and $\xi_1=\xi_{PS}$, the kinetic energy of the system is expressed as

$$T=\frac{4}{3}\rho L^4H\dot{\lambda}_{PS}^2+\frac{4}{3}\rho L^2H^3\frac{\dot{\lambda}_{PS}^2}{\lambda_{2p}^2\lambda_{PS}^4}, \tag{17}$$

and the potential is gained as

$$\Pi=8HL^2\left[\frac{\mu^\alpha}{2}\left(\lambda_{PS}^2+\lambda_{2p}^2+\lambda_{2p}^{-2}\lambda_{PS}^{-2}-3\right)\right.$$
$$+\frac{\mu^\beta}{2}\left(\lambda_{PS}^2\xi_{PS}^{-2}+\lambda_{PS}^{-2}\xi_{PS}^2-2\right)-\frac{P}{4HL}\lambda_{PS}$$
$$\left.-\frac{P_{2p}}{4HL}\lambda_{2p}-\frac{\varepsilon}{2}E^2\lambda_{2p}^2\lambda_{PS}^2\right], \tag{18}$$

where P_{2p} denotes the force in y-direction which is used to constrain the stretch as $\lambda_2=\lambda_{2p}$. For the reason that the inertia force in y-direction is 0 ($\dot{\lambda}_2=0$), thus, the constrained stress in y-direction, $P_{2p}\lambda_{2p}/(4HL)$, can be related to E as[23]

$$\frac{P_{2p}}{4HL}\lambda_{2p}=\mu^\alpha\left(\lambda_{2p}^2-\lambda_{PS}^{-2}\lambda_{2p}^{-2}\right)+\mu^\beta\left(1-\lambda_{PS}^{-2}\xi_{PS}^2\right)$$
$$-\varepsilon E^2\lambda_{PS}^2\lambda_{2p}^2. \tag{19}$$

Inserting Eq. (19) into Eq. (18), we can obtain

$$\Pi=8HL^2\left[\frac{\mu^\alpha}{2}\left(\lambda_{PS}^2-\lambda_{2p}^2+3\lambda_{2p}^{-2}\lambda_{PS}^{-2}-3\right)\right.$$
$$+\frac{\mu^\beta}{2}\left(\lambda_{PS}^2\xi_{PS}^{-2}+3\lambda_{PS}^{-2}\xi_{PS}^2-4\right)-\frac{P}{4HL}\lambda_{PS}$$
$$\left.+\frac{\varepsilon}{2}E^2\lambda_{2p}^2\lambda_{PS}^2\right]. \tag{20}$$

Substituting Eqs. (17) and (20) into the Euler-Lagrange equation (2), we obtain the governing equation under pure shear state

$$\ddot{\lambda}_{PS}-\frac{2\lambda_{2p}^{-2}}{\lambda_{PS}(\lambda_{2p}^{-2}+L^2H^{-2}\lambda_{PS}^4)}\dot{\lambda}_{PS}^2+\frac{3}{\rho H^2(\lambda_{2p}^{-2}+L^2H^{-2}\lambda_{PS}^4)}$$
$$\times\left[\mu^\alpha\left(\lambda_{PS}^5-3\lambda_{2p}^{-2}\lambda_{PS}\right)+\mu^\beta\left(\lambda_{PS}^5\xi_{PS}^{-2}-3\lambda_{PS}\xi_{PS}^2\right)\right.$$
$$\left.-\frac{P}{4HL}\lambda_{PS}^4+\varepsilon E^2\lambda_{2p}^2\lambda_{PS}^5\right]=0. \tag{21}$$

The rate of deformation in x-direction due to the dashpot under the pure shear state can be simplified by Eqs. (5) and (6) as

$$\frac{d\xi_{PS}}{dt} = \frac{\mu^{\beta}}{6\eta}\left(2\lambda_{PS}^{2}\xi_{PS}^{-1} - \xi_{PS} - \lambda_{PS}^{-2}\xi_{PS}^{3}\right). \quad (22)$$

III. NUMERICAL SIMULATION

Subject to a time-dependent voltage $\phi(t)$, the dynamic response of a DE membrane is very complicated.[28–36] In the following, by applying a sinusoidal electric load $E = E_0 \sin(2\pi ft)$, the dynamic characteristic of a visco-elastic DE membrane under the three different conditions is simulated, where f is the frequency of the applied electric field, and E_0 is the amplitude of the normal electric field. The initial condition is given by $\lambda_i(0) = \xi_i(0) = 1$ and $\dot{\lambda}_i(0) = 0$ due to the assumption that the system is activated from the reference configuration.[29,36] In the following calculations, we set the parameters for the application at $H = 1.0 \times 10^{-3}$m, $L = 5.0 \times 10^{-3}$m, $\rho = 1.2 \times 10^{3}$kg/m^3, $\varepsilon = 6.198 \times 10^{-11}$F/m,[29] $\mu^{\alpha} = 1.8 \times 10^{4}$Pa, $\mu^{\beta} = 4.2 \times 10^{4}$Pa, $\tau_v = 400$s.[37]

A. A DE membrane under equal-biaxial force

The effects of the equal-biaxial force P and the amplitude of the normal electric field E_0 on the frequency-dependent amplitude of λ_{EB} are shown in Fig. 4. For a given constant $E_0 = 1\times10^3$ kV/m, the largest peak is 0.05206 for $P = 0.2$ N, which happens at 431 Hz (black curve in Fig. 4(a)), and the amplitude attains much bigger values of 0.1248 for $P = 0.5$ N, which appears at 385 Hz (red curve in Fig. 4(a)) and 0.2373 for $P = 0.8$ N, which emerges at 340 Hz (blue curve in Fig. 4(a)). Compared to the effect of the force P, the amplitude of the normal electric field E_0 has a relatively minor influence on amplitude-frequency response in Fig. 4(b). Under an unchanging $P = 0.5$ N, the simulation results reveal that the peak amplitude changes from 0.1248 at 385 Hz for $E_0 = 1\times10^3$ kV/m (black curve in Fig. 4(b)) to 0.7120 at 371 Hz for $E_0 = 5\times10^3$ kV/m (blue curve in Fig. 4(b)). In all, increase in the equal-biaxial force P and the amplitude of the normal electric field E_0 reduces the resonant frequency (in this article, we define the frequency where the amplitude-frequency curve peaks as the resonant frequency) and enlarges the amplitude of vibration. The similar results induced by enlargement of external force and actuation voltage were also reported in the research of DE electromechanical resonator previously.[32,47]

When the equal-biaxial force $P = 0.5$ N and the amplitude of the normal electric field $E_0 = 5\times10^3$ kV/m, Fig. 5 illustrates the time-dependent behaviors of the vibration for three values of the excitation frequencies. Here, we choose the resonant frequency $f = 371$ Hz, half value of the resonant frequency $f = 185$ Hz, and double value of the resonant frequency $f = 742$ Hz. Figs. 5(c) and 5(d) indicate that the DE system under equal-biaxial force vibrates most strongly and exhibits beating[29,30,36] when the excitation frequency is around the resonant frequency ($f = 371$ Hz), which does not exist at $f = 185$ Hz (Fig. 5(b)) and $f = 742$ Hz (Fig. 5(f)). It can be found the deformation of ξ_{EB} is relatively small (Figs. 5(a), 5(c), and 5(e)), resulting from a big value of the visco-elastic relaxation time, which is consistent with our previous work done by Sheng *et al.*[36] It can be inferred that ξ_{EB} will increase gradually and is approaching to λ_{EB} if sufficient time is provided.

Figure 6 plots the phase diagrams and the Poincaré maps of λ_{EB} for the three different exitation frequencies $f = 185$ Hz, $f = 371$ Hz, and $f = 742$ Hz, while $P = 0.5$ N and $E_0 = 5\times10^3$ kV/m. As seen that the phase paths in Figs. 6(a)–6(c) are all presented in closed loops, indicating a stable vibration under the condition of equal-biaxial force. The stability transition can be better explained by the Poincaré maps[29,30,35,36] in Figs. 6(d)–6(f). The Poincaré maps for the three frequencies all form the closed loops, showing that the DE system under equal-biaxial force experiences a stable nonlinear quasi-periodic vibration.

B. A DE membrane under uniaxial force

Figure 7 displays the amplitude of λ_{UA1} as a function of the excitation frequency considering the effects of the uniaxial force P and the amplitude of the normal electric field E_0. When $E_0 = 1\times10^3$ kV/m is maintained, the amplitude peaks at 455 Hz with a value of 0.07724 for $P = 0.2$ N (black curve in Fig. 7(a)), and peaks at 438 Hz with a level of 0.1827 for $P = 0.5$ N (red curve in Fig. 7(a)), and a much larger peak with a value of 0.3079 for $P = 0.8$ N, appears at 425 Hz (blue curve in Fig. 7(a)). We also compare the effect of the amplitude of the normal electric field E_0 on amplitude-frequency response shown in Fig. 7(b). For an invariable value of $P = 0.5$ N, similar to the condition of equal-biaxial force, the amplitude of the normal electric field E_0 affects the resonant frequency of the system weakly. When E_0 increases from 1×10^3 kV/m to 5×10^3 kV/m, the peak amplitude increases from 0.1827 at 438 Hz (black curve in Fig. 7(b)) to 0.4897 at 424 Hz (blue curve in Fig. 7(b)). In summary, addition of the

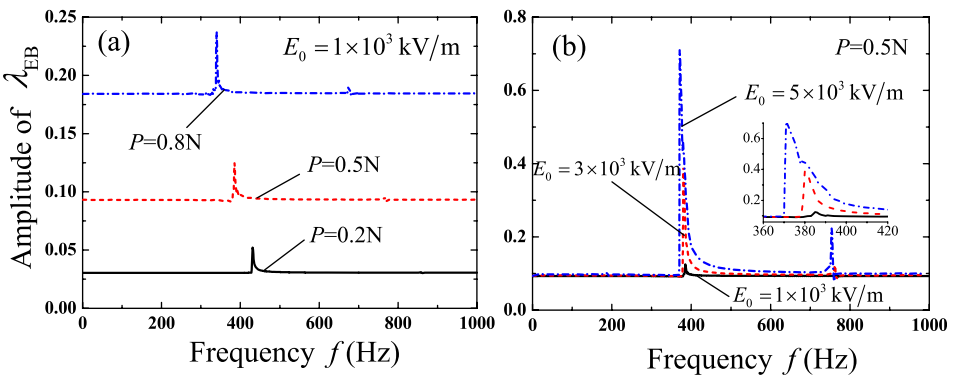

FIG. 4. Amplitude-frequency response of a DE membrane under equal-biaxial force. (a) Comparison of the frequency-dependent amplitude of λ_{EB} between the equal-biaxial force $P = 0.2$ N, $P = 0.5$ N, and $P = 0.8$ N with a constant $E_0 = 1\times10^3$ kV/m. (b) Comparison of the frequency-dependent amplitude of λ_{EB} between the amplitude of the normal electric field $E_0 = 1\times10^3$ kV/m, $E_0 = 3\times10^3$ kV/m, and $E_0 = 5\times10^3$ kV/m with a constant $P = 0.5$ N.

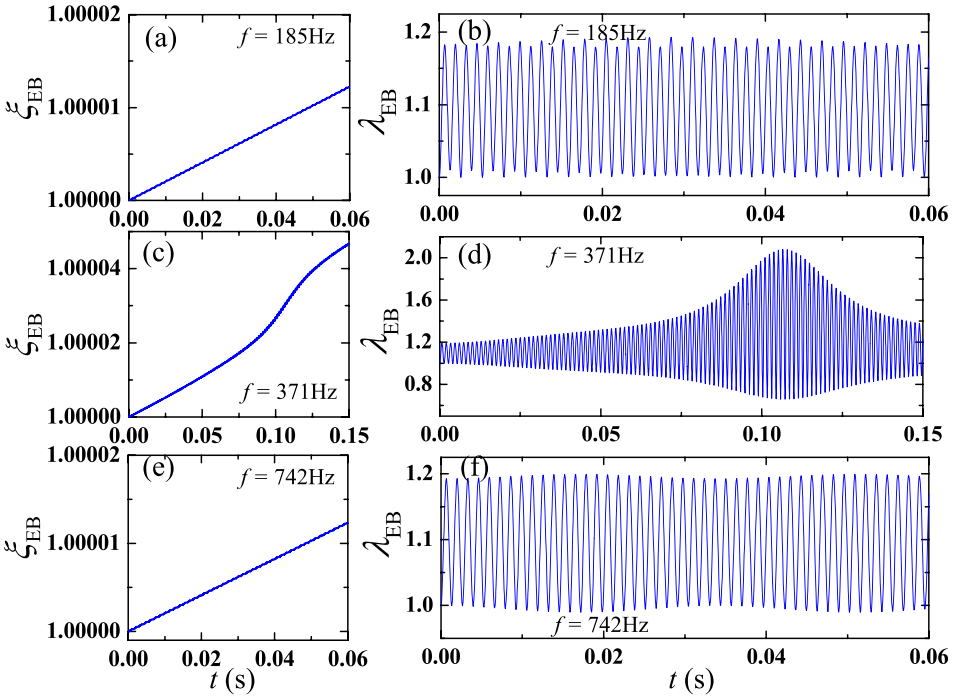

FIG. 5. The time-dependent behaviors of ξ_{EB} and λ_{EB} for three values of the excitation frequencies: (a) and (b) $f = 185$ Hz, (c) and (d) $f = 371$ Hz, (e) and (f) $f = 742$ Hz under $P = 0.5$ N and $E_0 = 5\times10^3$ kV/m.

uniaxial force P and the amplitude of the normal electric field E_0 decreases the resonant frequency and increases the amplitude of vibration, which is consistent with the condition of equal-biaxial force and the corresponding work reported before.[32,47] Particularly, the DE membrane under uniaxial force resonates at several frequencies and the amplitude-frequency response of the DE system appears multiple modes of vibration. When the frequency of excitation is close to one of the resonant frequencies, the corresponding vibration mode can be induced. This similar phenomenon of multiple modes was also reported by Zhu *et al.*[28]

Figure 8 inllustrates the time history of vibration for three values of the excitation frequencies with the uniaxial force $P = 0.5$ N and the amplitude of the normal electric field $E_0 = 5\times10^3$ kV/m. Similarly, we also choose the resonant frequency $f = 424$ Hz, half value of the resonant frequency $f = 212$ Hz, and double value of the resonant frequency $f = 848$ Hz. Unlike the DE system under the equal-biaxial force, the dynamic response of the DE system under uniaxial force exhibits strong nonlinearity when the excitation frequency is close to the resonant frequency, as shown in Fig. 8(d). The nonlinearity also shows more obvious when the excitation frequency is close to the half and double values of the resonant frequency, as shown in Figs. 8(b) and 8(f). Furthermore, same to the condition of equal-biaxial force, the DE system under uniaxial force reveals a big beating when the excitation frequency is close to the resonant frequency $f = 424$ Hz (Fig. 8(d)), which does not exist at $f = 212$ Hz (Fig. 8(b)) and $f = 848$ Hz (Fig. 8(f)). The reason of the small deformation of ξ_{UA1} (Figs. 8(a), 8(c), and 8(e)) is also due to the big value of viscoelastic relaxation time.

Figure 9 displays the phase diagrams and the Poincaré maps of λ_{UA1} for the three different exitation frequencies $f = 212$ Hz, $f = 424$ Hz, and $f = 848$ Hz, while $P = 0.5$ N and $E_0 = 5\times10^3$ kV/m. The phase paths in Figs. 9(a)–9(c) appear as the tangle of interlaced curves, indicating the system processes very complicated nonlinear behavior, which is consisitent to the time-history curve of λ_{UA1} shown in Figs. 8(b), 8(d), and 8(f). The Poincaré maps in Figs. 9(d)–9(f) are employed to detect the feature of the system and explain the

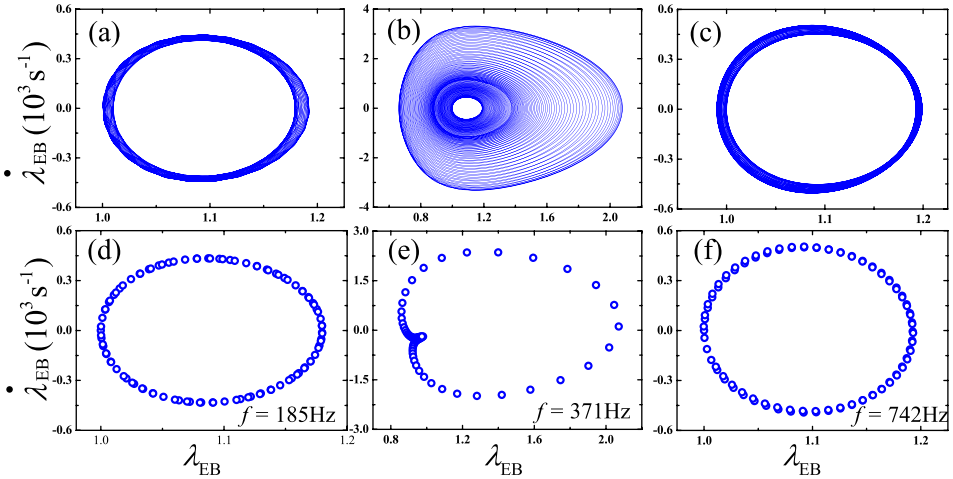

FIG. 6. Phase diagrams and Poincaré maps of the DE membrane under equal-biaxial force with $P = 0.5$ N and $E_0 = 5\times10^3$ kV/m for the three different exitation frequencies: (a) and (d) $f = 185$ Hz, (b) and (e) $f = 371$ Hz, (c) and (f) $f = 742$ Hz.

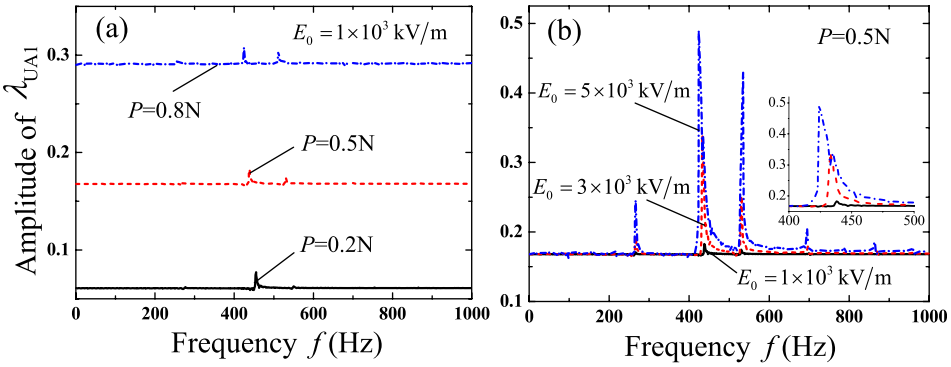

FIG. 7. Amplitude-frequency response of a DE membrane under uniaxial force. (a) Comparison of the frequency-dependent amplitude of λ_{UA1} between the uniaxial force $P = 0.2$ N, $P = 0.5$ N, and $P = 0.8$ N with a constant $E_0 = 1 \times 10^3$ kV/m. (b) Comparison of the frequency-dependent amplitude of λ_{UA1} between the amplitude of the normal electric field $E_0 = 1\times10^3$ kV/m, $E_0 = 3 \times 10^3$ kV/m, and $E_0 = 5\times10^3$ kV/m with a constant $P = 0.5$ N.

stability transition.[29,30,35,36] All the Poincaré maps for the three frequencies are disordered and do not form the closed loops, showing that the DE system under the uniaxial tensile forces experiences an aperiodic vibration.[29,30,36] The results demonstrate that the dynamic performance of the DE system under uniaxial forces is aperiodic and relatively unstable, compared with the unstable static performance with the incidental pull-in instability.[23,24]

C. A DE membrane under pure shear state

Figure 10 describes the amplitude of λ_{PS} as a function of the excitation frequency considering the effects of the force P, the amplitude of the normal electric field E_0, and the constrained stretch λ_{2p}. Under the unchanging $E_0 = 3\times10^3$ kV/m and $\lambda_{2p} = 2$, a large peak of the amplitude-frequency appears around 381 Hz with a value of 1.2271 for $P = 0.1$ N (black curve in Fig. 10(a)), and a much larger peak with a value of 1.2854 for $P = 0.3$ N appears at 366 Hz (red curve in Fig. 10(a)), the largest amplitude for $P = 0.5$ N peaks at 351 Hz with a value of 1.3139 (blue curve in Fig. 10(a)). Then the effect of the amplitude of the normal electric field E_0 on amplitude-frequency response is investigated (Fig. 10(b)). For the invariable values of $P = 0.1$ N and $\lambda_{2p} = 2$, different with the conditions of equal-biaxial force and uniaxial force, the increase in E_0 adds up the resonant frequency of the pure-shear DE system slightly (from 381 Hz to 391 Hz). As E_0 increases from 3×10^3 kV/m to 5×10^3 kV/m, the peak amplitude increases from 1.2271 at 381 Hz (black curve in Fig. 10(b)) to very large values (red and blue curves in Fig. 10(b)). As reported by Zhu *et al.*,[33] the peak amplitude of the resonant frequency can be even unbounded when the voltage increases, which is consistent with our present results. In the following, we explore the effect of the constrained stretch λ_{2p} on the amplitude-frequency response with $P = 0.1$ N and $E_0 = 3\times10^3$ kV/m. When λ_{2p} increases from 2 to 3 and 4, the resonant frequency increases slightly (from 381 Hz to 391 Hz and 401 Hz), and the peak value of the amplitude also enlarges from 1.2271 ($f = 381$ Hz, black curve in Fig. 10(c)) to very large values (red and blue curves in Fig. 10(c)), which is similar to the effect of E_0. However, when the actuation frequency is kept away from the resonant frequency, enlargement of λ_{2p} induces a reduction of the value of the amplitude, as illustrated in Fig. 10(c). The reason may be a larger prestretch in y-direction suppresses the deformation in x-direction, causing a reduction of the amplitude

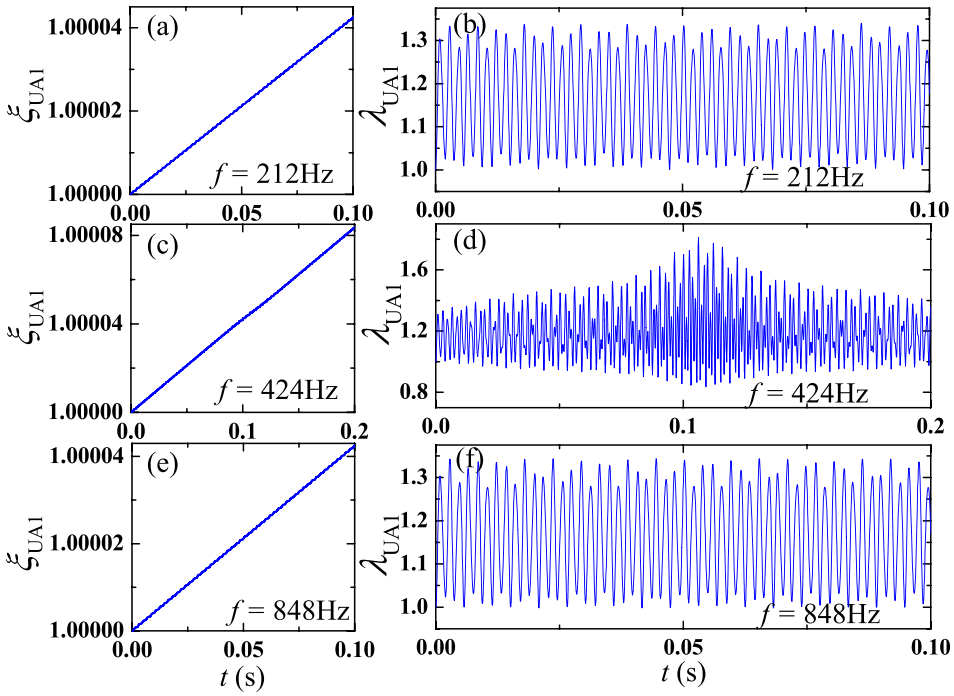

FIG. 8. The time-dependent behavior of ξ_{UA1} and λ_{UA1} for three values of the excitation frequencies: (a) and (b) $f = 212$ Hz, (c) and (d) $f = 424$ Hz, (e) and (f) $f = 848$ Hz under $P = 0.5$ N and $E_0 = 5\times10^3$ kV/m.

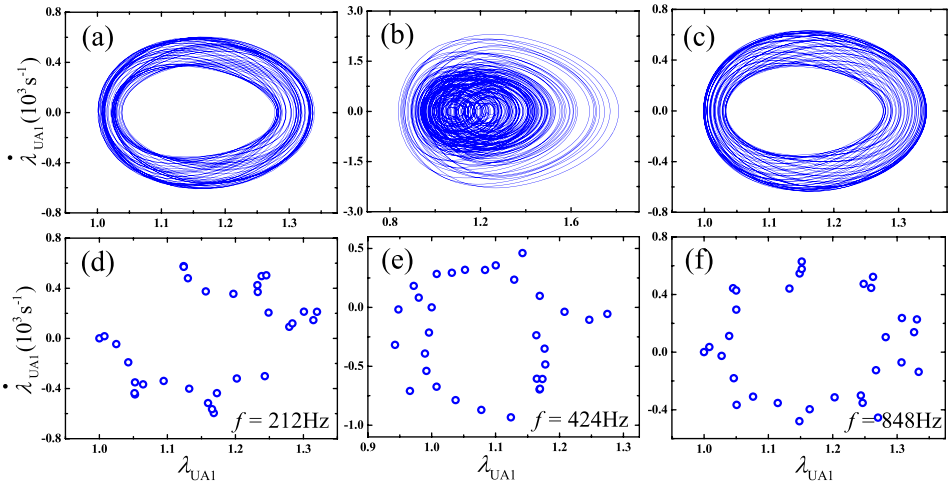

FIG. 9. Phase diagrams and Poincaré maps of the DE membrane under unixial force with $P = 0.5$ N and $E_0 = 5 \times 10^3$ kV/m for the three different exitation frequencies: (a) and (d) $f = 212$ Hz, (b) and (e) $f = 424$ Hz, (c) and (f) $f = 848$ Hz.

when the excitation frequency is away from resonant frequency. To sum up, enlargement of the force P decreases the resonant frequency and adds up the amplitude of vibration, the reason is similar to that explained before. However, inconsistent with the conditions of equal-biaxial force and uniaxial force, increase in E_0 augments both the resonant frequency and the amplitude of vibration. The reason may be the plus sign before the electrostatic energy in Eq. (21), comparing the minus sign before the electrostatic energy in Eq. (9), and Eqs. (13) and (14) under the conditions of equal-biaxial force and uniaxial force, respectively. Increase in the constrained stretch λ_{2p} adds up the resonant frequency and the peak amplitude when the excitation frequency is close to the resonant frequency, while decreases the amplitude when the excitation frequency is away from the resonant frequency. The reason why the enlargement of λ_{2p} adds up the resonant frequency (which is different with the force P in x-direction) may be that addition of λ_{2p} causes the increase in the constrained force P_{2p} in y-direction.

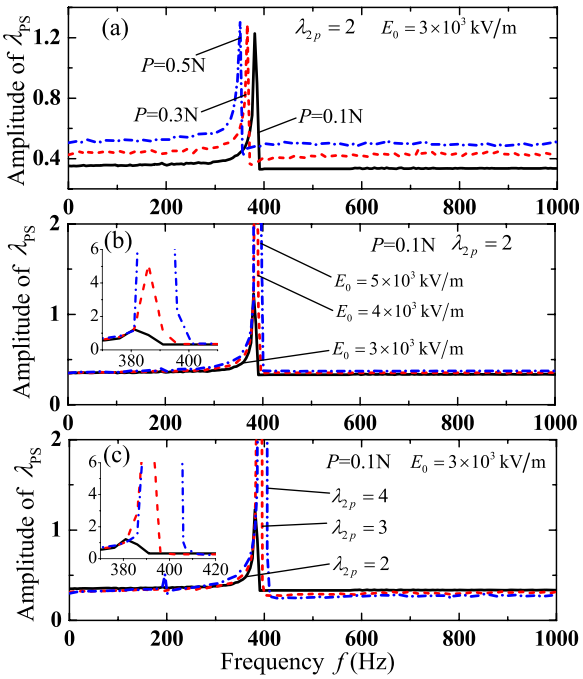

FIG. 10. Amplitude-frequency response of a DE membrane under pure shear state. (a) Comparison of the frequency-dependent amplitude of λ_{PS} between the force $P = 0.1$ N, $P = 0.3$ N, and $P = 0.5$ N with the constant $E_0 = 3\times10^3$ kV/m and $\lambda_{2p} = 2$. (b) Comparison of the frequency-dependent amplitude of λ_{PS} between $E_0 = 3\times10^3$ kV/m, $E_0 = 4\times10^3$ kV/m, and $E_0 = 5\times10^3$ kV/m with the constant $P = 0.1$ N and $\lambda_{2p} = 2$. (c) Comparison of the frequency-dependent amplitude of λ_{PS} between $\lambda_{2p} = 2$, $\lambda_{2p} = 3$, and $\lambda_{2p} = 4$ with the constant $P = 0.1$ N and $E_0 = 3\times10^3$ kV/m.

Figure 11 inllustrates the time history of the vibration for three values of the excitation frequencies under pure shear state with $\lambda_{2p} = 2$, $P = 0.1$ N, and $E_0 = 3\times10^3$ kV/m. Similarly, to study the effect of excitation frequency, here we choose the resonant frequency $f = 381$ Hz, half value of the resonant frequency $f = 190$ Hz, and double value of the resonant frequency $f = 762$ Hz. The same to a DE under equal-biaxial force, the DE system of pure shear state vibrates most strongly and demonstrates a beating when the excitation frequency is close to the resonant frequency $f = 381$ Hz (Fig. 11(d)), which does not exist at $f = 190$ Hz (Fig. 11(b)) and $f = 762$ Hz (Fig. 11(f)). The reason of the small deformation of ξ_{PS} (Figs. 11(a), 11(c), and 11(e)) is same to that explained before, that is, due to the big value of viscoelastic relaxation time.

Figure 12 plots the phase diagrams and the Poincaré maps of λ_{PS} for the three different exitation frequencies $f = 190$ Hz, $f = 381$ Hz, and $f = 762$ Hz under the condition of $\lambda_{2p} = 2$, $P = 0.1$ N, and $E_0 = 3\times10^3$ kV/m. The phase paths are all presented in closed loops shown in Figs. 12(a)–12(c), declaring a stable vibration under the pure shear state. The Poincaré maps in Figs. 12(d)–12(f) can be used to describe the stability transition better.[29,30,35,36] The Poincaré maps for the three frequencies all form the closed loops, showing that the DE system under pure shear state undergoes a stable nonlinear quasi-periodic vibration.

IV. CONCLUSION

By using the Euler-Lagrange equation, we developed the dynamic model for homogeneously deformed viscoelastic DE actuator under three different conditions of mechanical load: equal-biaxial force, uniaxial force, and pure shear state. Numerical results demonstrated that when the DE membrane was under the boundary of equal-biaxial force, the resonant frequency reduced and the maximal amplitude increased with the enlargement of the mechanical

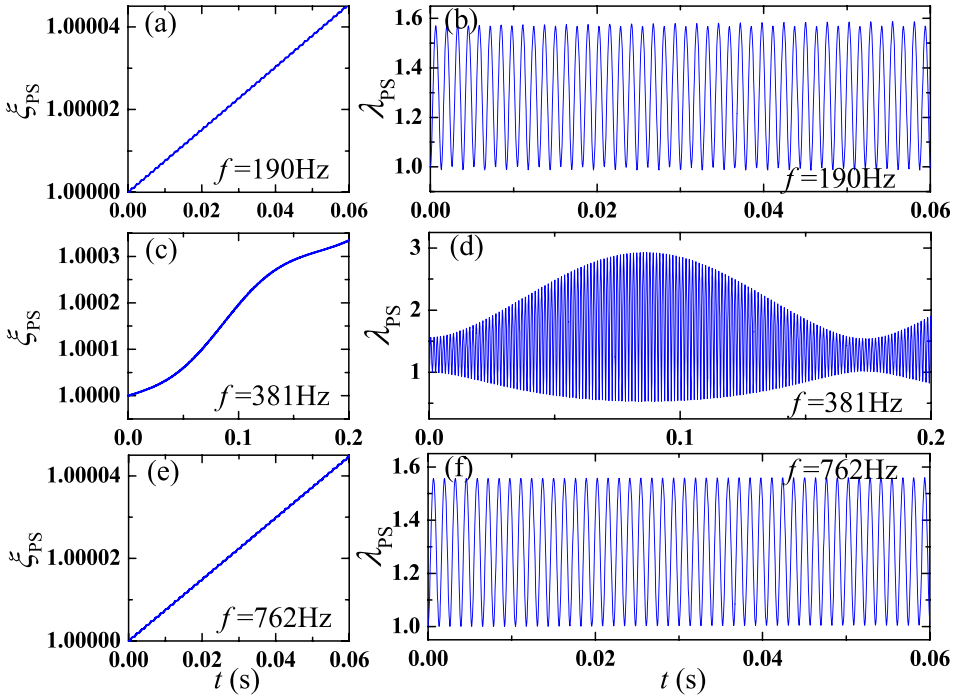

FIG. 11. The time-dependent behavior of ξ_{PS} and λ_{PS} for three values of the excitation frequencies: (a) and (b) $f = 190$ Hz, (c) and (d) $f = 381$ Hz, (e) and (f) $f = 762$ Hz under $\lambda_{2p} = 2$, $P = 0.1$ N, and $E_0 = 3\times10^3$ kV/m.

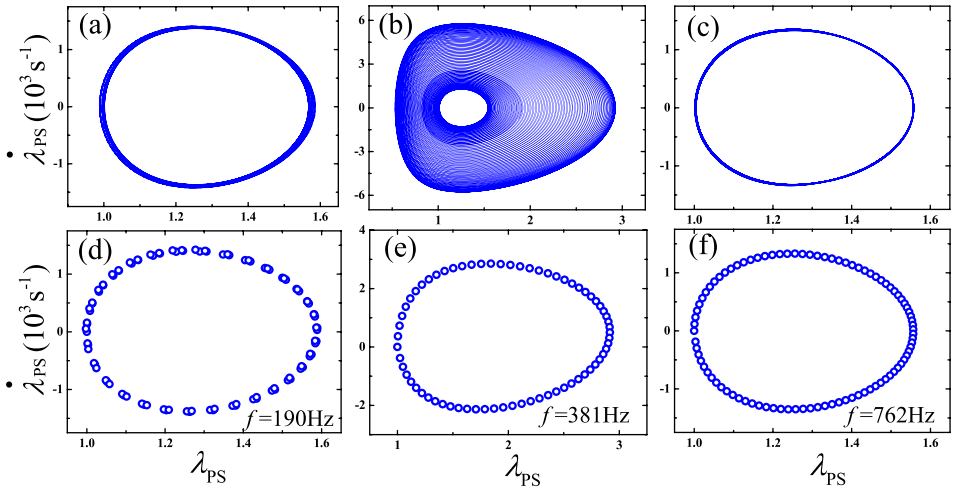

FIG. 12. Phase diagrams and Poincaré maps of the DE membrane under pure shear state with $\lambda_{2p} = 2$, $P = 0.1$ N, and $E_0 = 3\times10^3$ kV/m for the three different exitation frequencies: (a) and (d) $f = 190$ Hz, (b) and (e) $f = 381$ Hz, (c) and (f) $f = 762$ Hz.

load and the applied electric field. The time dependent behavior of the stretch indicated that a beating occurred near the resonant frequency. The phase diagrams and the Poincaré maps detected the feature of the equal-biaxially tensile DE system a nonlinear quasi-periodic vibration. Under the condition of uniaxial force, the DE membrane appeared as a phenomenon of mutiple modes of vibration. Diminution of the resonant frequency and increase in maximal amplitude were caused by the magnification of mechanical force and electric field. The time-history curve revealed a beating when the excitation frequencies were next to resonant frequency. An aperiodic motion of the uniaxially tensile DE system was certified by the phase paths and the Poincaré maps. When the DE membrane was under pure shear state (a certain direction was constrained), the amplitude-frequency response declared that growing values of mechanical load decreased the resonant frequency and added up the maximal amplitude, while increase in applied electric field enlarged both the resonant frequency and the maximal amplitude. Furthermore, enlargement of the constrained stretch adds up the resonant frequency and the peak amplitude when the excitation frequency is close to the resonant frequency, while decrease the amplitude when the excitation frequency is kept away from the resonant frequency. Similar to the state of equal-biaxial force, under the pure-shear mode, the stretch-time response showed a beating near the resonant frequency, and the phase diagrams and the Poincaré maps at several specific excitation frequencies implied a nonlinear quasi-periodic motion. The results can help to determine the applied deformation mode to be better used for DE actuators based on the corresponding dynamic response and dynamic stability.

ACKNOWLEDGMENTS

This research was supported by the Doctoral Fund of the Ministry of Education of China (Grant No. 20120201110030) and the Foundation for Innovative Research Groups of the

National Natural Science Foundation of China (Grant No. 11321062). J. Zhang was supported by the China Scholarship Council to study as a visiting student at UCLA.

[1]R. Pelrine, R. Kornbluh, Q. Pei, and J. Joseph, Science **287**, 836 (2000).
[2]F. Carpi, S. Bauer, and D. De Rossi, Science **330**, 1759 (2010).
[3]P. Brochu and Q. Pei, Macromol. Rapid Commun. **31**, 10 (2010).
[4]L. Di Lillo, A. Schmidt, D. A. Carnelli, P. Ermanni, G. Kovacs, E. Mazza, and A. Bergamini, J. Appl. Phys. **111**, 024904 (2012).
[5]Z. Suo, Acta Mech. Solida Sin. **23**, 549 (2010).
[6]I. A. Anderson, T. A. Gisby, T. G. Mckay, B. M. O'Brien, and E. P. Calius, J. Appl. Phys. **112**, 041101 (2012).
[7]Q. Pei, M. Rosenthal, S. Stanford, H. Prahlad, and R. Pelrine, Smart Mater. Struct. **13**, N86 (2004).
[8]Q. Pei, R. Pelrine, S. Stanford, R. Kornbluh, and M. Rosenthal, Synth. Met. **135–136**, 129 (2003).
[9]R. Shankar, T. K. Ghosh, and R. J. Spontak, Soft Matter **3**, 1116 (2007).
[10]G. Kovacs, L. Düring, S. Michel, and G. Terrasi, Sens. Actuators A **155**, 299 (2009).
[11]S. Rosset, M. Niklaus, P. Dubois, and H. R. Shea, J. Microelectromech. Syst. **18**, 1300 (2009).
[12]F. Carpi, G. Frediani, S. Turco, and D. De Rossi, Adv. Funct. Mater. **21**, 4002 (2011).
[13]T. Lu, S. Cai, H. Wang, and Z. Suo, J. Appl. Phys. **114**, 104104 (2013).
[14]S. Shian, R. M. Diebold, and D. R. Clarke, Opt. Express **21**, 8669 (2013).
[15]C. Keplinger, J.-Y. Sun, C. C. Foo, P. Rothemund, G. M. Whitesides, and Z. Suo, Science **341**, 984 (2013).
[16]T. McKay, B. O'Brien, E. Calius, and I. Anderson, Appl. Phys. Lett. **97**, 062911 (2010).
[17]J. Huang, S. Shian, Z. Suo, and D. R. Clarke, Adv. Funct. Mater. **23**, 5056 (2013).
[18]R. Kaltseis, C. Keplinger, R. Baumgartner, M. Kaltenbrunner, T. Li, P. Machler, R. Schwodiauer, Z. Suo, and S. Bauer, Appl. Phys. Lett. **99**, 162904 (2011).
[19]S. Plante and S. Dubowsky, Int. J. Solid Struct. **43**, 7727 (2006).
[20]M. Kollosche, J. Zhu, Z. Suo, and G. Kofod, Phys. Rev. E **85**, 051801 (2012).
[21]X. Zhao and Z. Suo, Phys. Rev. Lett. **104**, 178302 (2010).
[22]L. Liu, Y. Liu, and J. Leng, J. Appl. Phys. **112**, 033519 (2012).
[23]T. Lu, J. Huang, C. Jordi, G. Kovacs, R. Huang, D. R. Clarke, and Z. Suo, Soft Matter **8**, 6167 (2012).
[24]B. Li, H. Chen, and J. Zhou, Appl. Phys. A **110**, 59 (2013).
[25]P. Dubois, S. Rosset, M. Niklaus, M. Dadras, and H. Shea, J. Microelectromech. Syst. **17**, 1072 (2008).
[26]J. Fox and N. Goulbourne, J. Mech. Phys. Solids **56**, 2669 (2008).
[27]K. Hochradel, S. Rupitsch, A. Sutor, R. Lerch, D. K. Vu, and P. Steinmann, Appl. Phys. A **107**, 531 (2012).
[28]J. Zhu, S. Cai, and Z. Suo, Int. J. Solid Struct. **47**, 3254 (2010).
[29]B.-X. Xu, R. Mueller, A. Theis, M. Klassen, and D. Gross, Appl. Phys. Lett. **100**, 112903 (2012).
[30]J. Sheng, H. Chen, B. Li, and Y. Wang, Smart Mater. Struct. **23**, 045010 (2014).
[31]C. Feng, L. Jiang, and W. M. Lau, J. Micromech. Microeng. **21**, 095002 (2011).
[32]T. Li, S. Qu, and W. Yang, Int. J. Solid Struct. **49**, 3754 (2012).
[33]J. Zhu, S. Cai, and Z. Suo, Polym. Int. **59**, 378 (2010).
[34]J. Zhang and H. Chen, Int. J. Smart Nano Mater. **5**, 76 (2014).
[35]H. Yong, X. He, and Y. Zhou, Int. J. Eng. Sci. **49**, 792 (2011).
[36]J. Sheng, H. Chen, L. Liu, J. Zhang, Y. Wang, and S. Jia, J. Appl. Phys. **114**, 134101 (2013).
[37]C. C. Foo, S. Cai, S. J. A. Koh, S. Bauer, and Z. Suo, J. Appl. Phys. **111**, 034102 (2012).
[38]C. C. Foo, S. J. A. Koh, C. Keplinger, R. Kaltseis, S. Bauer, and Z. Suo, J. Appl. Phys. **111**, 094107 (2012).
[39]J. Zhang, H. Chen, J. Sheng, L. Liu, Y. Wang, and S. Jia, Appl. Phys. A **116**, 59 (2014).
[40]J. Zhang, H. Chen, and B. Li, Europhys. Lett. **108**, 57002 (2014).
[41]J. Zhou, L. Jiang, and R. E. Khayat, J. Appl. Phys. **115**, 124106 (2014).
[42]W. Hong, J. Mech. Phys. Solids **59**, 637 (2011).
[43]H. Wang, M. Lei, and S. Cai, J. Appl. Phys. **113**, 213508 (2013).
[44]J. Zhang, Y. Wang, D. McCoul, Q. Pei, and H. Chen, Appl. Phys. Lett. **105**, 212904 (2014).
[45]C. Keplinger, M. Kaltenbrunner, N. Arnold, and S. Bauer, Appl. Phys. Lett. **92**, 192903 (2008).
[46]R. Huang and Z. Suo, Proc. R. Soc. London, Ser. A **468**, 1014 (2012).
[47]B. Li, J. Zhang, L. Liu, H. Chen, S. Jia, and D. Li, J. Appl. Phys. **116**, 124509 (2014).